Curvature-Induced Asymmetric Spin-Wave Dispersion

Otálora, A. S.; Yan, M.; Schultheiss, H.; Hertel, R.; Kákay, A.;

Originally published:

November 2016

Physical Review Letters 117(2016), 227203

DOI: https://doi.org/10.1103/PhysRevLett.117.227203

Perma-Link to Publication Repository of HZDR:

https://www.hzdr.de/publications/Publ-24431

Curvature induced asymmetric spin-wave dispersion

Jorge A. Otálora

Departamento de Física, Universidad Técnica Federico Santa María, Avenida España 1680, Casilla 110-V, Valparaíso, Chile and Departamento de Física, Universidad Santiago de Chile and CEDENNA, Avda. Ecuador 3493, Santiago, Chile

Ming Yan

Department of Physics, Shanghai University, 99 Shangda Road, BaoShan District, Shanghai 200444, China

Helmut Schultheiss

Helmholtz-Zentrum Dresden - Rossendorf, Institute of Ion Beam Physics and Materials Research, Bautzner Landstr. 400, 01328 Dresden, Germany and Technische Universität Dresden, D-01062 Dresden, Germany

Riccardo Hertel

Karlsuhe Institute of Technology, Physikalisches Institut, Wolfgang-Gaede-Str. 1, D-76131 Karlsruhe, Germany and Institut de Physique et Chimie des Matériaux de Strasbourg, UMR 7504, CNRS, and Université de Strasbourg, 23 rue du Loess, F-67300 Strasbourg, France

Attila Kákay*

Helmholtz-Zentrum Dresden - Rossendorf, Institute of Ion Beam Physics and Materials Research, Bautzner Landstr. 400, 01328 Dresden, Germany

(Dated: September 11, 2016)

Abstract

In magnonics, spin waves are conceived as electron-charge free information carriers. Their wave behaviour have stand them as the key elements to achieve lower power consumption, faster operative rates and better packings in magnon-based computational technologies. Hence, knowing alternative ways that reveals certain properties of their undulatory motion is an important task. Here, we show using micromagnetic simulations and analytical calculations that spin-wave propagation in ferromagnetic nanotubes is fundamentally different than in thin films. The dispersion relation is asymmetric regarding the sign of the wave vector. It is a purely curvature induced effect and its fundamental origin is identified to be the classical dipole-dipole interaction. The analytical expression of the dispersion has the same mathematical form as in thin-films with Dzyalonshiinsky-Moriya interaction. Therefore, this curvature induced effect can be seen as a "dipole-induced Dzyalonshiinsky-Moriya-like" effect.

Using the electron's spin degree of freedom for data processing instead of its charge is one of the grand challenges. The first success story can nowadays be seen in spintronic devices employing various magneto-resistance effects in magnetic sensors and storage applications. About ten years ago a new research field called *magnonics* emerged driven by the idea to use magnons as carrier of spin information [1–7]. Magnons, also called spin waves (SWs), are the dynamic eigen-oscillations of the spin system in ferromagnets with frequencies between GHz to THz range and with nanometer wavelengths. Novel materials allow for coherent propagation of SWs over mesoscopic distances without any charge transport involved, paving the way for green data processing. Many concepts have been proposed theoretically and experimentally, leading to prototype building blocks of a spin-wave-based logic [8–13]. The experimental discovery of novel phenomena such as spin Hall effect, Dzyaloshinski-Moria-Interaction [14, 15] (DMI), spin Seebeck effect and others proved as powerful mechanisms to excite, manipulate and detect SWs in thin magnetic films on the nanometer scale via coupling the magnons to charge and heat transport. One particular feature of SWs in thin films is very intriguing: A certain set of SWs known as Damon-Eshbach [16] modes show a non-reciprocity regarding inversion of the wave vector caused by dipolar interaction. When the propagation direction is reversed, these magnons switch from the top to the bottom surface of the thin film. Very recently it was discovered, that an asymmetric exchange interaction (DMI) in ultra-thin ferromagnetic films can also cause an asymmetric SW dispersion [17], *i.e.*, one can switch from positive to negative dispersion upon reversal of the wave vector. In this Letter we show that one can obtain a similar asymmetric SW dispersion purely caused by dipolar interaction when going from thin films to three dimensional structures with curved surfaces, in particular magnetic nano-tubes (MNT). Such novel structures can nowadays be very well produced[18, 19] motivated by the broad range of applications for magnetoresistive devices, optical meta materials, cell/DNA separators and drug delivery vectors [20, 21]. The high stability of their equilibrium state [22, 23] against external perturbations, and their robust domain walls propagating with velocities faster than the SW phase velocity [24], promote MNTs as appealing candidates for racetrack memory devices [25, 26] and information processing [24, 27].

In this Letter, we report the numerical simulation and full analytical description of curvature-induced asymmetric SW dispersion in nanotubes, which has the same mathematical form [28–31] as the DMI but identifies the dipole-dipole interaction as the origin

of the asymmetry. We demonstrate that the degree of asymmetry can be tuned with the tube geometry but also with small electric currents flowing through the nanotube. Besides the tuneability, contrary to thin-films with DMI the asymmetry is present and is significant even in the absence of external magnetic fields.

Finite element micromagnetic simulations [32, 33] were performed to study the propagation of SWs in MNTs. The numerical research is focused on a tube defined by the outer radius $R = 30$ nm, wall thickness $d = 10$ nm and length $L = 4$ μm. The MNT is assumed to be made of Permalloy and the following material parameters are used, saturation magnetisation $\mu_0 M_s = 1$ T, exchange stiffness constant $A = 1.3 \times 10^{-11}$ J/m, negligible magnetocrystalline anisotropy ($K_u = 0$) and low Gilbert damping $\alpha_G = 0.01$. Details of simulations are presented in the Supplementary materials S1.

Propagation and dispersion of SWs in MNTs are simulated for an equilibrium state in which the magnetisation rotates around the circumference of the tube, thus forming a perfect flux closure configuration [34, 35]. This state in the following is referenced as a vortex (V) configuration. It is not a ground state for the given geometry and an external field is required to stabilise it. A circular Oersted field, $H_0 \geq H_{\text{crit}}$, induced by a current flowing through the MNT or its core can serve this function. The critical field for the nanotube with the described geometry is $\mu_0 H_{\text{crit}} = 53$ mT [36].

A schematics of the considered system is shown in Figure 1a with the tube in the V state together with the polar coordinate system used throughout the manuscript, being ρ, φ and z, the radial, azimuthal and long axis coordinates. The SWs are excited with a homogeneous rf-field applied in the radial direction at the middle of the tube in a 100 nm wide region, as indicated with an orange ring in Figure 1a. The SWs propagate from the middle of the nanotube toward its ends with a wave vector k_z. The circulation direction of the magnetisation $\hat{\varphi}$ together with the propagation direction $\hat{z}$ defines a chirality or handedness. The direction of propagation is shown on all Figures such, that SWs propagating to right (left) with $k_R \equiv +|k_z|$ ($k_L \equiv -|k_z|$) define the right (left) handed (RH and LH) chirality. Since the propagation direction is perpendicular to the magnetization, similarly to thin films this excitation geometry is addressed as Damon-Eshbach geometry.

The SW excitation and propagation were simulated for several values of the circular field. For all field values, the continuous rf-field exciting SWs is applied as long as the steady state is reached. Figure 1b shows a snapshot in time of the SW profiles for three

different excitation frequencies, for 8, 10 and 20 GHz, for a circular field of 80 mT, well above the critical field. The colour scheme represents the radial component of the magnetisation in an unrolled view. The rf-field position is illustrated with an orange bar. λ_L and λ_R denote the wave length of the SWs on the left and right of the excitation region, respectively. Remarkably, the wave length of the SWs propagating to left differs from those propagating to right. This difference in the wave length decreases with increasing excitation frequencies, but never vanishes, according to the micromagnetic simulations for the considered range of frequencies.

Figure 2 shows the SW dispersion obtained from the micromagnetic simulations for two different values of the circular field, 80 mT and 1 T. The dispersion is asymmetric regarding the propagation direction and moreover, the minimum of the dispersion depends on the circular field as seen by comparing Figure 2a with 2b. Despite the geometrical similarity, our simulations show that DE modes in nanotubes behave differently than its thin-film counterparts. Simulations suggest, that for $k_z = k_L$ there is a range of wave vectors wherein the group velocity is negative, specific to Backward Volume (BV) modes in thin-films. Similar effect has been recently reported for thin-films with Dzyalonshinskii-Moriya interaction [17, 28–31].

For a deeper understanding on the origin of the asymmetry observed in simulations, an analytical formula of the SW dispersion of nanotubes is presented. The analytical description is given under the frame of micromagnetic continuum-theory. The dispersion relation is calculated by: (i) linearising the Landau-Lifshitz-Gilbert (LLG) equation, and (ii) solving the linear equation in terms of individual magnons with wave vector k_z along the nanotube axis $\hat{z}$, an integer wave number n characteristic of the azimuthal symmetry along $\hat{\varphi}$, and with eigenfrequency $\omega_n(k_z)$. An extensive analytical derivation presented in details in Ref. [37] (guidelines can also be found in the Supplementary materials S2) leads the following dispersion relation for the coherently distributed SWs ($n = 0$; SWs with planar wave mode profiles as shown in fig. 1b) along the $\hat{\varphi}$ axis:

$$\frac{\omega_0(k_z)}{\gamma_0 \mu_0 M_s} = \mathcal{K}_0(k_z) + \sqrt{\mathcal{A}_0(k_z)\mathcal{B}_0(k_z)} \tag{1}$$

where the quantities $\mathcal{A}_0$ and $\mathcal{B}_0$ are defined as:

$$\begin{aligned}\mathcal{A}_0(k_z) &= l_{ex}^2\left(k_z^2 - \frac{1}{b^2}\right) + h_0 + \mathcal{L}_0(k_z),\\ \mathcal{B}_0(k_z) &= l_{ex}^2 k_z^2 + h_0 + \mathcal{J}_0(k_z),\end{aligned} \tag{2}$$

being the functions $\mathcal{J}_0$, $\mathcal{K}_0$ and $\mathcal{L}_0$ given as

$$\begin{aligned}\mathcal{J}_0(k_z) &= \frac{\pi}{S}\int_0^\infty dk \frac{k^3}{2\left(k^2+k_z^2\right)}\left(\Gamma_0(k)\right)^2\\ \mathcal{K}_0(k_z) &= \frac{\pi}{S}\int_0^\infty dk \frac{k^2 k_z}{k^2+k_z^2}\Gamma_0(k)\Lambda_0(k)\\ \mathcal{L}_0(k_z) &= \frac{\pi}{S}\int_0^\infty dk \frac{2kk_z^2}{k^2+k_z^2}\left(\Lambda_0(k)\right)^2\end{aligned} \tag{3}$$

with $\Lambda_0(k) = \int_r^R d\rho\ \rho J_0(k\rho)$, $\Gamma_0(k) = -2\Lambda_1(k)$, $J_0(x)$ the First Kind Bessel Functions of zero order, $b^{-2} = 2\pi\ln(R/r)/S$ and $S = \pi(R^2 - r^2)$ the nanotube cross section, with R and r being the outer and inner radii, respectively. The $l_{ex} = \sqrt{A/K_d}$ is the exchange length, A the exchange stiffness constant, $K_d = (1/2)\mu_0 M_s^2$ the shape anisotropy constant, and h_0 the circular field normalised to the saturation magnetisation M_s.

Figures 2a and b show the dispersion calculated with Equation 1. The solid line representing the analytical calculations is in a perfect agreement with the results of the simulations.

Using Equation 1, the SW dispersion is calculated for tubes with different diameter and varying circular field. Two cases are summarised for tubes with 10 nm film thickness and outer radius of 30 and 150 nm in Figure 3a and b, respectively. As shown, the minima of the dispersion is shifted towards larger k_z values with increasing circular field, allowing for the manipulation of the asymmetry and the wave vector ranges for which the SWs have negative group velocity. However, the asymmetry is decreased with increasing outer diameter, since the curvature is reduced and completely vanishes for infinite diameters at the thin film limit. It is noteworthy to mention, that equation 1 allows for a systematic study of the eigenoscillations and its features $(k_z, \omega_0(k_z))$ in function of nanotubes size, material parameters, applied circular and/or axial fields, without the need for the expensive micromagnetic simulations.

The asymmetric SW dispersion reported in this Letter cannot be explained within the classical frame of the DE dispersion known for thin films. The DE modes in nanotubes with negative k_z behave as the volume charge free BV modes in thin films. Such effect, however is already known for thin films [17] with antisymmetric exchange (DMI) due to spin-orbit coupling. In fact the DMI favours a canting of the spins with a given chirality and therefore

introduces a local symmetry break which can lead to an asymmetric dispersion relation [28–31]. Nevertheless, for nanotubes the source of the asymmetric dispersion resides only in the dipole-dipole interaction and which is discussed in the following.

Note, that equation 1 has the same mathematical form as in thin-films with interfacial DMI or in crystals with a special symmetry (C_{nv}) and bulk DMI (see Eqs. 6 - 9 in Ref. Di *et al.* [30] and Table 1 in Ref. Cortés-Ortuño and Landeros [28]). The $\mathcal{K}_0(k_z)$ plays the same role in nanotubes as the well-known asymmetrical terms in thin-films(crystals) with interfacial(bulk) DMI (*i.e.* the term $\frac{2\gamma_0}{M_s}Dk$ in the dispersion of thin-films with interfacial DMI [30], where D is the DMI constant) but with the difference that $\mathcal{K}_0(k_z)$ originates from the dynamic volume charges created by the SWs as a result of the tubular curvature. From equation 3 it is easy to see that $\mathcal{K}_0(k_z)$ is an odd function (*i.e.*, $\mathcal{K}_0(k_z) = -\mathcal{K}_0(-k_z)$), therefore being the asymmetrical term in the dispersion relation.

The term $\mathcal{K}_0(k_z)$, which can only be calculated by numerical integration of the corresponding Bessel functions, comprises the dynamic dipolar energy arising from the surface as well as from the volume charges[38] $\rho_V \equiv -(M_s/4\pi)\nabla \cdot \vec{M}$. **The negative dispersion or negative group velocity, however should be related to small or close to zero volume charges.** With the magnetisation in the vortex state for a SW with wave vector k_z, wave number $n = 0$ and eigenfrequency ω, the volume charges averaged over the nanotube radius is $\langle \rho_V \rangle = \langle \rho_V \rangle_0 \, e^{i(k_z z - \omega t + \xi)}$, with:

$$\langle \rho_V \rangle_0 = -\frac{M_s^2}{4\pi} \left(\frac{1}{\bar{\rho}} + k_z \sqrt{\frac{\mathcal{B}_0(k_z)}{\mathcal{A}_0(k_z)}} \right) \left(1 + \frac{\mathcal{B}_0(k_z)}{\mathcal{A}_0(k_z)} \right)^{-\frac{1}{2}} \tag{4}$$

where $\mathcal{A}_0(k_z)$ and $\mathcal{B}_0(k_z)$ are defined in Eq. 2; ξ is the phase constant of the radial and axial SW components. It can be seen, that the amplitude is proportional to two terms. The first term, $1/\bar{\rho}$ being the inverse of the nanotube average radius which is proportional to the mean nanotube curvature [39]. The second term $k_z\sqrt{\frac{\mathcal{B}_0(k_z)}{\mathcal{A}_0(k_z)}}$ depends on the propagation vector k_z. Hence, the sum of the two terms depends on the sign of k_z. Therefore, for opposite propagation directions the dynamic volume charges are different.

In figure 4a the volume charge amplitude as a function of the wave vector is shown for NTs with three different radius. As expected from the previous considerations, it has an asymmetric dependence on the k_z. Moreover, zero volume charges are obtained for k_z values different from zero. Around these k_z

values the reduction in energy from the surface charges is larger than the energy increase from the volume charges, thus the total energy decreases, leading to a negative dispersion.

In figure 4d the SW profile as well as the divergence calculated with our TetraMag [32, 33] code is shown for a case when the SWs propagating towards the opposite ends have the same wave length. Clearly, the resulting dynamic volume charges and thus the dipolar energies differ for the two sides. In experiments (or simulations) the excitation is done with a well defined frequency, therefore the SW's should possess the same energy for the opposite travel directions. In NTs this can only be reached if the wave lengths differ such, that the dynamic dipolar energy resulting from the surface and volume charges is the same for the two propagation directions. As a consequence SWs propagating to opposite directions have different wave length and show an asymmetric dispersion. It is worth mentioning that the dipole-dipole interaction was reported to be also responsible for the asymmetric domain wall propagation in nanotubes [40].

The SW asymmetry defined as the frequency difference of the SWs traveling to opposite direction but with the same wave vector is also proportional to the asymmetrical term and can be calculated analytically using Eq. 1. It reads as:

$$\Delta f = \frac{\gamma M_s}{2\pi}\left|\omega_0(k_\mathrm{z}) - \omega_0(-k_\mathrm{z})\right| = \frac{\gamma M_s}{\pi}|\mathcal{K}_0(k_\mathrm{z})|. \tag{5}$$

The SW asymmetry can be estimated from equation 3 by looking at the dependence of $\mathcal{K}_0(k_\mathrm{z})$ on the value of k_z. Equation 5 in function of the wave vector is plotted for nanotubes with different radius in figure 4b. It can be seen that the maximum frequency difference decreases with increasing tube radius. For tubes with small diameter this value is in the range of several GHz, however, for tubes with 500-600 nm in diameter – that are accessible experimentally due to the recent progress in material science [18] – the frequency difference is still in the range of several 100's of MHz. The SW wave length for which the maximum asymmetry is reached is shown in Figure 4c as a function of the nanotube outer radius. It is in perfect agreement with our simple predictions based on the volume charges, namely the asymmetry (smallest contribution to of the volume charges to the total energy) is largest for wave lengths comparable to the nanotube diameter.

In a final step two limiting cases of the dispersion are presented: 1) $k_z = 0$ **and 2)** $k_z \gg 1/R$**. For** $k_z = 0$ **the dispersion has the following form** $\omega_{\mathbf{FMR}} =$

$\gamma_0\mu_0\sqrt{(H_0 - H_u)(H_0 + M_s)}$ **which resemble the Kittel Formulae for Ferromagnetic Resonance (FMR) of a thin-film with in-plane magnetization parallel to the applied field, and both oriented perpendicular to an in-plane easy axis of the shape anisotropy field** H_u**. For large radius,** $H_u \ll H_0$**, therefore the well-known FMR Formulae [41]** $\omega_{\mathbf{FMR}} \approx \gamma_0\mu_0\sqrt{H_0(H_0 + M_s)}$ **for thin-films with a homogeneous in-plane magnetization parallel to the applied magnetic field** H_0 **is obtained.**

For very small wave length, $k_z \gg 1/R$**, the dispersion can be written as:**

$$\omega_0(k_z) \approx \gamma_0\mu_0\sqrt{(M_s l_{ex}^2 k_z^2 - H_u + H_0 + M_s)(Dk_z^2 + H_0)}, \tag{6}$$

which is identical to the exchange-dominated dispersion relation of a planar thin-film in Damon-Esbach configuration with in-plane magnetization oriented perpendicularly to the in-plane easy axis [16, 42] (The derivation of the asymptotic analytical expressions are summarised in Ref. [37]).

In summary, we have shown using micromagnetic simulations as well as analytical calculations that SW propagation in nanotubes is fundamentally different than in thin films. The observed asymmetric dispersion is a purely curvature induced effect[43–45] and can be tuned with small electrical currents. We have shown that the SW asymmetry is in the range of MHz to GHz in frequency and depends on the nanotube radius. The analytical expression of the dispersion has the same mathematical form as in thin-films with Dzyalonshiinsky-Moriya interaction. The fundamental origin of the asymmetric dispersion is the classical dipole-dipole interaction, therefore it can be seen as a "dipole induced DMI-like effect". We hope that the presented results will encourage the experimental verification of the presented curvature induced effect.

Financial support by the Centers of Excellence with BASAL/CONICYT financing, GRANT FB0807, CEDENNA and FONDECYT REGULAR GRANT 1161403 is gratefully acknowledged. A.K. would like to acknowledge for the helpful discussions with J. Lindner and J. Fassbender. M.Y. is supported by the National Natural Science Foundation of China (No. 11374203) and Shanghai Key Laboratory of High Temperature Superconductors (No. 14DZ2260700). Also, authors are very grateful with R. Gallardo for fruitful discussions.

* Corresponding author: a.kakay@hzdr.de

[1] V. Kruglyak and R. Hicken, J. Magn. Magn. Mater. **306**, 191 (2006).

[2] S. Neusser and D. Grundler, Advanced Materials **21**, 2927 (2009).

[3] A. Khitun, M. Bao, and K. L. Wang, J. Phys. D: Appl.Phys. **43**, 264005 (2010).

[4] V. V. Kruglyak, S. O. Demokritov, and D. Grundler, J. Phys. D: Appl. Phys. **43**, 264001 (2010).

[5] D. Grundler, Nat. Phys. **11**, 438 (2015).

[6] B. Lenk, H. Ulrichs, F. Garbs, and M. Münzenberg, Phys. Rep. **507**, 107 (2011).

[7] A. V. Chumak, V. I. Vasyuchka, A. A. Serga, and B. Hillebrands, Nat. Phys. **11**, 453 (2015).

[8] R. Hertel, W. Wulfhekel, and J. Kirschner, Phys. Rev. Lett. **93** (2004).

[9] A. V. Chumak, A. A. Serga, and B. Hillebrands, Nat. Commun. **5** (2014).

[10] K. Vogt, F. Y. Fradin, J. E. Pearson, T. Sebastian, S. D. Bader, B. Hillebrands, A. Hoffmann, and H. Schultheiss, Nat. Commun. **5** (2014).

[11] K. Wagner, A. Kákay, K. Schultheiss, A. Henschke, T. Sebastian, and H. Schultheiss, Nat. Nano. **11**, 432 (2016).

[12] S. Urazhdin, V. E. Demidov, H. Ulrichs, T. Kendziorczyk, T. Kuhn, J. Leuthold, G. Wilde, and S. O. Demokritov, Nat. Nano. **9**, 509 (2014).

[13] A. Haldar, D. Kumar, and A. O. Adeyeye, Nat. Nano. **11**, 437 (2016).

[14] I. Dzyaloshinsky, Journal of Physics and Chemistry of Solids **4**, 241 (1958).

[15] T. Moriya, Phys. Rev. **120**, 91 (1960).

[16] R. Damon and J. Eshbach, Journal of Physics and Chemistry of Solids **19**, 308 (1961).

[17] K. Zakeri, Y. Zhang, J. Prokop, T.-H. Chuang, N. Sakr, W. X. Tang, and J. Kirschner, Phys. Rev. Lett. **104**, 137203 (2010).

[18] K. Nielsch, F. Castaño, S. Matthias, W. Lee, and C. Ross, Adv. Eng. Mater. **7**, 217 (2005).

[19] M. Vázquez, *Magnetic Nano- and Microwires, 1st Edition* (Elsevier, 2016).

[20] D. F. Emerich and C. G. Thanos, Expert Opinion on Biological Therapy **3**, 655 (2003).

[21] S. J. Son, J. Reichel, B. He, M. Schuchman, and S. B. Lee, Journal of the American Chemical Society **127**, 7316 (2005).

[22] R. Streubel, L. Han, F. Kronast, A. A. Ünal, O. G. Schmidt, and D. Makarov, Nano Letters

14, 3981 (2014).

[23] A. Buchter, R. Wölbing, M. Wyss, O. F. Kieler, T. Weimann, J. Kohlmann, A. B. Zorin, D. Rüffer, F. Matteini, G. Tütüncüoglu, F. Heimbach, A. Kleibert, A. Fontcuberta i Morral, D. Grundler, R. Kleiner, D. Koelle, and M. Poggio, Phys. Rev. B **92**, 214432 (2015).

[24] M. Yan, C. Andreas, A. Kákay, F. García-Sánchez, and R. Hertel, Appl. Phys. Lett. **99**, 122505 (2011).

[25] S. S. P. Parkin, M. Hayashi, and L. Thomas, Science **320**, 190 (2008).

[26] M. Hayashi, L. Thomas, R. Moriya, C. Rettner, and S. S. P. Parkin, Science **320**, 209 (2008).

[27] J. A. Otálora, J. A. López-López, P. Vargas, and P. Landeros, Appl. Phys. Lett. **100**, 072407 (2012).

[28] D. Cortés-Ortuño and P. Landeros, J. Phys.: Cond. Matter **25**, 156001 (2013).

[29] F. Ma and Y. Zhou, RSC Adv. **4**, 46454 (2014).

[30] K. Di, V. L. Zhang, H. S. Lim, S. C. Ng, M. H. Kuok, J. Yu, J. Yoon, X. Qiu, and H. Yang, Phys. Rev. Lett. **114**, 047201 (2015).

[31] Y. Iguchi, S. Uemura, K. Ueno, and Y. Onose, Phys. Rev. B **92**, 184419 (2015).

[32] R. Hertel, in *Handbook of Magnetism and Advanced Magnetic Materials* (John Wiley & Sons, Ltd, 2007) pp. 1003–1020.

[33] A. Kákay, E. Westphal, and R. Hertel, IEEE Trans. Magn. **46**, 2303 (2010).

[34] P. Landeros, S. Allende, J. Escrig, E. Salcedo, D. Altbir, and E. Vogel, Appl. Phys. Lett. **90**, 102501 (2007).

[35] P. Landeros, O. J. Suarez, A. Cuchillo, and P. Vargas, Phys. Rev. B **79**, 024404 (2009).

[36] J. Otálora, D. Cortés-Ortuño, D. Görlitz, K. Nielsch, and P. Landeros, J. Appl. Phys. **117**, 173914 (2015).

[37] J. A. Otálora, M. Yan, H. Schultheiss, R. Hertel, and A. Kákay, submitted to Phys. Rev. B.

[38] W. F. Brown, *Micromagnetics* (Interscience Publishers, 1963).

[39] M. Berger, Chern: a great geometer of the 20th century , 184 (1992).

[40] M. Yan, C. Andreas, A. Kákay, F. García-Sánchez, and R. Hertel, Appl. Phys. Lett. **100**, 252401 (2012).

[41] C. Kittel, *Introduction to Solid State Physics*, 6th ed. (John Wiley & Sons, Inc., New York, 1986).

[42] B. Kalinikos and A. Slavin, J. Phys. C: Sol. State Phys. **19**, 7013 (1986).

[43] B. M. Tanygin, J. Magn. Magn. Mater. **323**, 616 (2011).

[44] R. Hertel, SPIN **3**, 1340009 (2013).

[45] O. V. Pylypovskyi, D. D. Sheka, V. P. Kravchuk, K. V. Yershov, D. Makarov, and Y. Gaididei, Scientific Reports **6**, 23316 (2016).

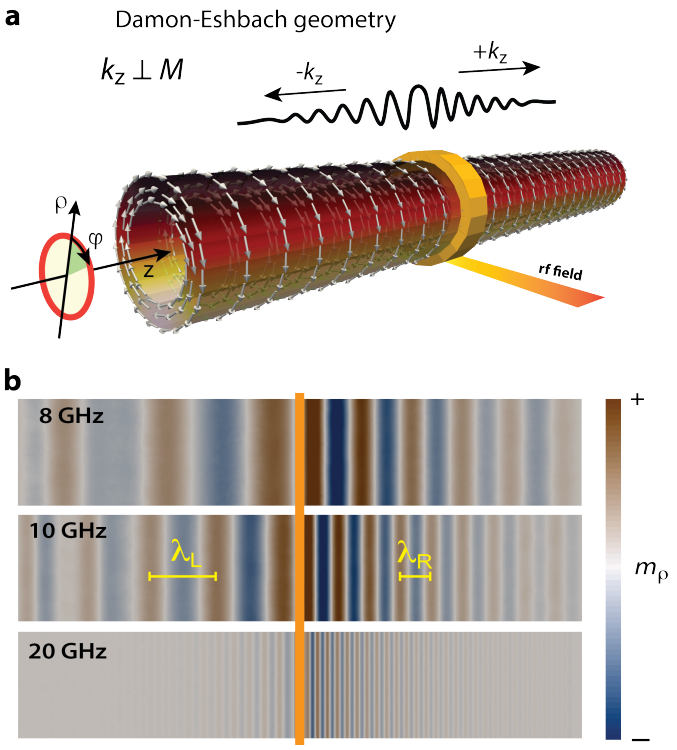

FIG. 1. **a)** Schematic illustration of a nanotube in a vortex state and the cylindrical coordinate system. SWs are excited in the middle with a radial rf field, as illustrated by the orange ring. The SWs travel toward the ends of the nanotube with a wave vector k_z perpendicular to the magnetisation. The $+k_z$ and $-k_z$ indicate the right and left propagation directions, respectively. **b)** A snapshot in time of the SW profiles (radial component of the magnetisation colour coded) for three different excitation frequencies, for 8, 10 and 20 GHz for a circular field of 80 mT. The orange bar indicates the position and width of the rf field. λ_L (λ_R) denotes the wave length of the waves traveling to the left (right).

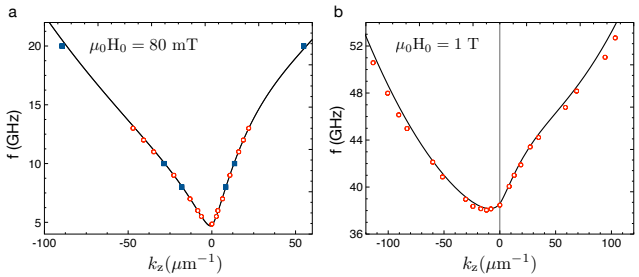

FIG. 2. SW dispersion relation obtained by micromagnetic simulations (red and blue dots) and analytical calculations (solid line) for circular fields of 80mT **a)** and 1T **b)**. The blue squares mark the frequencies for which the SW profile is shown in Figure 1b. A nearly perfect agreement between the results of micromagnetic simulations and analytical calculations is found.

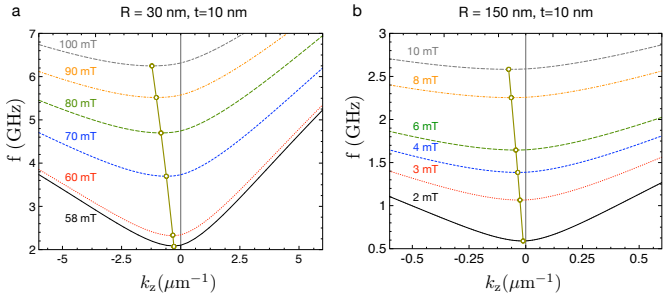

FIG. 3. The dispersion of SWs is summarised for several circular fields as a function of the wave number for nanotubes with **a)** 30 nm and **b)** 150 nm outer radius and 10 nm film thickness. The minima of the dispersion is shifted towards larger k_z values with increasing circular field for both diameters. The open dots represent the minima for each circular field and the solid line connecting them is a guide to the eye only.

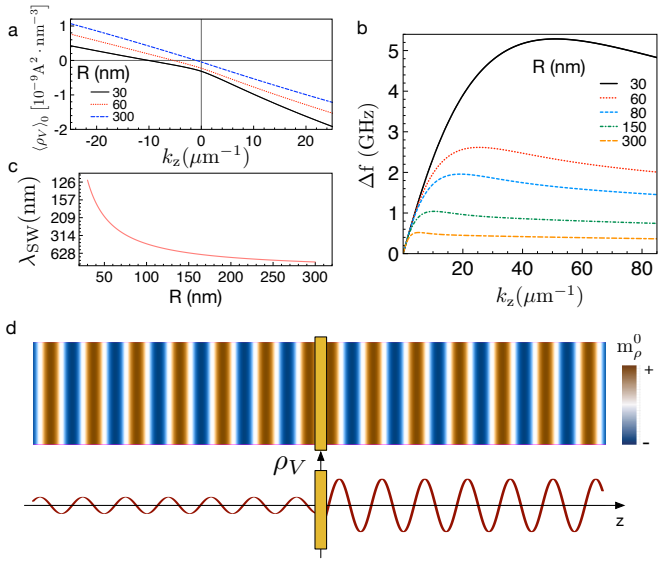

FIG. 4. **a)** The volume charge amplitude as a function of the wave vector. **b)** SW asymmetry in function of the wave vector k_z for nanotubes with varying radius. **c)** The wave length λ_{SW} of the excited SWs for which the maximum asymmetry is reached versus the nanotube radius. **d)** SW profile for waves with equal wave length but opposite travel direction and the corresponding volume charges. The colour scheme encodes the radial component of the dynamic magnetisation. The dark yellow rectangles mark the excitation region.